applied sciences

MDPI

Article

Study on Stiffness Parameters of the Hardening Soil Model in Sandy Gravel Stratum

Xiaomeng Shi [1,2,*], Jinglai Sun [3], Yi Qi [4,*], Xiangyang Zhu [5], Xueming Zhang [1,2], Ruisong Liang [4] and Hongjiang Chen [4]

1 Key Laboratory of Urban Underground Engineering of Ministry of Education, Beijing Jiaotong University, Beijing 100044, China
2 School of Civil Engineering, Beijing Jiaotong University, Beijing 100044, China
3 Beijing Municipal Engineering Research Institute, Beijing 100037, China
4 Beijing Urban Construction Group Co., Ltd., Beijing 100088, China
5 China Railway Engineering Design and Consulting Group Co., Ltd., Beijing 100073, China
* Correspondence: shixm@bjtu.edu.cn (X.S.); qiyi@mail.bucg.com (Y.Q.)

Abstract: Sandy gravel stratum is very common in tunnels and underground engineering projects. The accurate determination of mechanical parameters is crucial for engineering design and construction. The Hardening Soil (HS) Model, which accounts for both shear hardening and compression hardening, has demonstrated advantages in numerical simulations. This study conducts large-scale mechanical experiments, including triaxial drained shear tests, loading-unloading tests, and standard consolidation tests, on sandy gravel specimens. The results reveal that the ratio of the three stiffness parameters in the HS Model, namely Young's modulus under triaxial loading (E_{50}), oedometric loading (E_{oed}), and unloading-reloading (E_{ur}) is 1:1:4.3. The validity of the established stiffness ratio relationship is verified through numerical simulations of a foundation pit project and comparison with field monitoring data, demonstrating a consistent agreement between the simulation results and actual monitoring values.

Keywords: sandy gravel stratum; hardening soil model; stiffness parameters; Young's modulus; large-scale laboratory tests

check for updates

Citation: Shi, X.; Sun, J.; Qi, Y.; Zhu, X.; Zhang, X.; Liang, R.; Chen, H. Study on Stiffness Parameters of the Hardening Soil Model in Sandy Gravel Stratum. *Appl. Sci.* **2023**, *13*, 2710. https://doi.org/10.3390/app13042710

Academic Editor: Eduardo Ferreira da Silva

Received: 14 December 2022
Revised: 9 February 2023
Accepted: 10 February 2023
Published: 20 February 2023

1. Introduction

The sandy gravel stratum, characterized by a high concentration of coarse particles, presents challenges in obtaining accurate mechanical parameters through laboratory testing, thereby hindering the efficacy of numerical simulation in analyzing projects within these strata [1–3]. It is crucial to identify practical and reasonable parameters for engineering projects in the sandy gravel stratum. The results of a large-scale cyclic triaxial study conducted by Evans and Zhou on sandy soils with varying coarse grain contents demonstrated a correlation between the increase in shear modulus and the increase in coarse grain content [4]. Rollins et al. [5] found that the modulus normalization curve shifted progressively upward as the surrounding pressure increased. Particle size, permeability, direct shear, and compressive strength of coarse-grained soils were investigated by Cetin et al. [6]. Bassel et al. [7] used a large triaxial test on sand and gravel soil, focusing on the effect of the volume fraction of gravel, particle size, particle gradation, and initial stress state on the mechanical properties of gravel soil. Lirer et al. [8] explained the stress–strain characteristics of different granular materials of the same gradation in the elasto-plastic range, especially the effect of the static soil pressure coefficient on the static soil pressure in the compacted state.

In 1970, Duncan et al. [9] established a currently widely used incremental model of elasticity based on the hyperbolic stress–strain relationship proposed by Konder, namely the D-C principal model, which is also the most representative nonlinear elastic model.

Schzna et al. [10] introduced plasticity theory into the D-C model in 1998, and proposed a soil hardening model considering both shear hardening and compression hardening. The HS model is an advanced constitutive model for soils which belongs to the isotropic hardening elastic-plastic model [11–14]. It can accurately reflect the mechanical behavior of soil under loading and unloading [15]. The HS model has obvious advantages, as it can accurately describe the soil properties by inputting three Young's moduli: triaxial loading E_{50}, oedometric loading E_{oed}, and unloading-reloading E_{ur} [16–18].

E_{s1-2} is the compression modulus of soil commonly used in the geological report and is obtained from a 100 to 200 kPa loading test. Usually, E_{s1-2} equals E_{oed} [19,20]. However, the E_{50} and E_{ur} required for the HS model cannot be calculated. Therefore, establishing a geometric relationship between E_{s1-2} and the stiffness modulus of the HS model can simplify the value selection process of numerical simulation. These three parameters can usually be determined by laboratory tests. Many experts and scholars have studied the HS model parameters of clay and sand [21,22], as shown in Table 1.

Table 1. HS model key stiffness relationships for different soil types.

No.	Soil Type	E_{oed}:E_{50}:E_{ur}
1 [23]	Clay (Shanghai area)	1:1.3:5.7
2 [23]	Silty clay (Shanghai area)	1:1.1:3.9
3 [24]	Mucky soil (Ningbo area)	1:0.28:2.1
4 [24]	Silty clay (Ningbo area)	1:1:5
5 [25]	Granite residual soil (Shenzhen area)	1:2.1:7.6
6 [26]	Silty clay (Taipei area)	1:2.8:8.3
7 [27]	Lacustrine Clay	1:1:4
8 [28]	Glacial clays (Chicago)	1:1.5:6.25
9 [29]	Silt (the Yangtze river estuary)	1:1.2:5
10 [29]	Granite residual soil (Guangdong area)	1:2.7:8.3

Research on the HS model key stiffness relationship mainly focused on sandy soil, silty clay, and residual granite soil, with little research on coarse particles of soil like sandy gravel. One of the most important reasons is that the particle of sandy gravel has a large volume and high strength. It is difficult to directly obtain its soil constitutive parameters through conventional lab tests. This paper conducts large-scale mechanical experiments, including the triaxial drained shear test, the loading-unloading test, and the standard consolidation test on large-scale sandy gravel specimens. The objective of the experiment is to test the Young's modulus under triaxial loading (E_{50}), oedometric loading (E_{oed}), and unloading-reloading (E_{ur}), and analyze the proportional relationship of these parameters in the HS model. The results of the experiments are then utilized in a numerical simulation of a foundation pit project and compared with engineering monitoring data to validate the accuracy of the test outcomes.

2. Large-Scale Experiments of Sandy Gravel

2.1. Sandy Gravel Sample

Beijing has a wide range of thick sand and sandy gravel stratum. The construction of tunnels, foundation pits, and other underground projects often encounters the sandy gravel stratum. The sample was taken from 37 m underground of a subway station in Beijing. According to the geological survey report, the density of the undisturbed soil sample was 2.449 g/cm^3, the dry density was 2.436 g/cm^3, and the looseness coefficient was about 1.22. According to the geotechnical test specification, a gradation analysis of the sandy gravel soil sample was carried out. Three groups of sand gravel screening tests were conducted, and the results are shown in Table 2. The grading curve can be obtained based on the test results, as shown in Figure 1.

Table 2. Gradation of undisturbed sandy gravel (%).

Samples	Particle Size (mm)									
	60	40	20	10	5	2	1	0.5	0.25	0.075
1	100	100	59.74	32.55	24.56	20.21	16.95	13.95	3.49	0.55
2	100	100	58.45	40.17	31.64	18.77	19.31	14.33	4.12	0.84
3	100	100	60.58	46.35	29.51	20.84	16.78	9.73	2.71	0.89
Average value	100	100	59.59	39.69	28.57	19.94	17.68	12.67	3.44	0.76

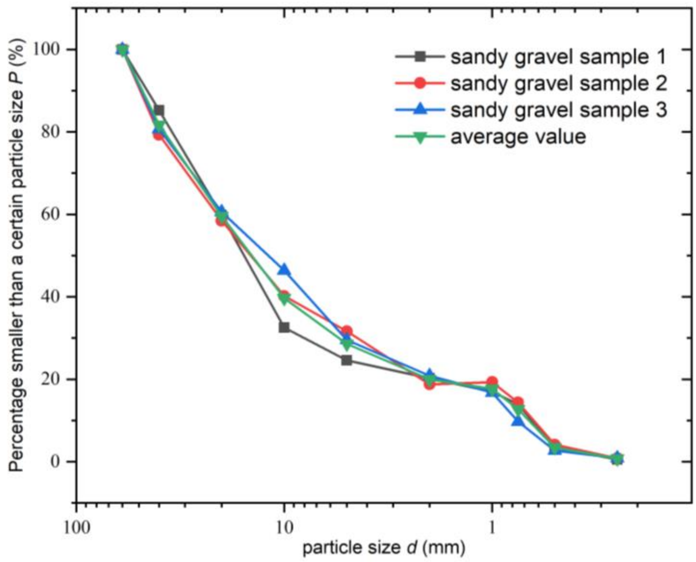

Figure 1. Undisturbed sandy gravel gradation curve.

C_u is the non-uniformity coefficient, and its value determines the uniformity of soil particle distribution, as shown in Equation (1). For the sandy gravel specimen in this test, C_u = 48.06 > 10, indicating that the particle size distribution was not concentrated and the uniformity was poor. C_C is the curvature coefficient, which determines the continuity of soil gradation, as shown in Equation (2). The C_C obtained in this test was 3.27, indicating that the continuity of soil was poor, and the content of coarse particles was high. In contrast, the content of fine particles was small, and the average particle size was about 21.7 mm.

$$C_u = d_{60}/d_{10} \tag{1}$$

$$C_c = \frac{d_{30}^2}{d_{10}d_{60}} \tag{2}$$

where d_{60} is the percentage smaller than 60 mm, d_{30} is the percentage smaller than 30 mm, and d_{10} is the percentage smaller than 10 mm, as shown in Figure 1.

2.2. Triaxial Compression Test

The Young's moduli of triaxial loading and unloading-reloading used in the HS model are usually determined by a triaxial consolidation drainage test when the confining pressure is 100 kPa. According to the stress–strain curve, the secant stiffness at 50% of the failure load is the reference value of triaxial loading Young's modulus E_{50}. When the unloading-reloading test is carried out during the triaxial test, the reference value of unloading-reloading modulus E_{ur} can be determined. The secant modulus is obtained by connecting the upper and lower points of the hysteretic circle, as shown in Figure 2.

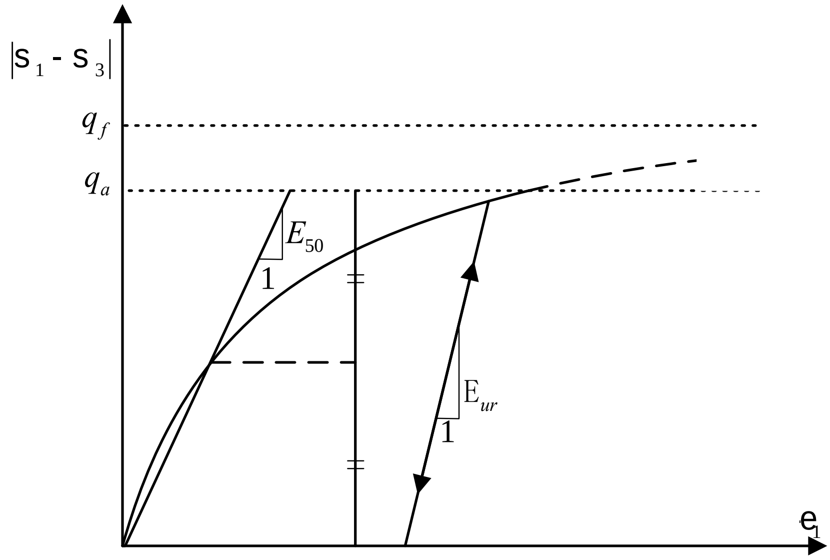

Figure 2. Stress–strain curve of E_{50} and E_{ur}.

This study used a large-scale testing machine to carry out the triaxial compression test, with a sample height of 600 mm and diameter of 300 mm. The maximum axial displacement of the testing machine can reach 150 mm, and the maximum axial pressure can be 250 kN, as shown in Figure 3.

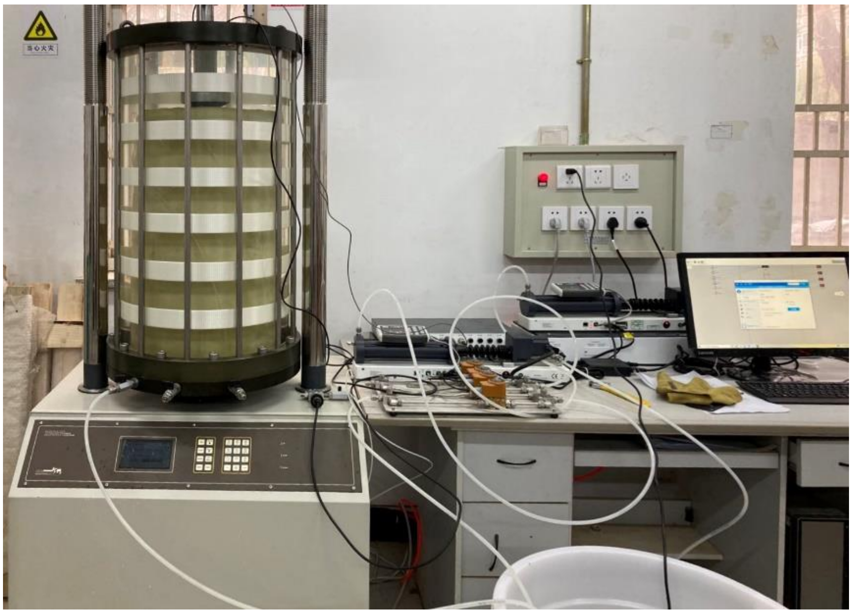

Figure 3. Large-scale triaxial compression testing machine.

The preparation of the sandy gravel soil sample presented unique challenges, as it differs from silt or cohesive soil in its large particle size, loose composition, sharp edges, and low cohesion. As a result, conventional sample preparation methods could not be utilized. In order to effectively prepare the sample for testing, it was loaded and compacted on the instrument base, as illustrated in Figure 4. The test density was carefully controlled based on the natural density of the soil mass specified in the geological survey report. The sample was then saturated and consolidated, prior to being loaded under a confining pressure of 100 kPa. During the loading process, care was taken to avoid a high shear rate, which could result in the full discharge of pore water. A shear rate of 0.1 mm/min was employed. Upon completion of a loading time of 900 min, the sample had achieved a cylindrical shape with a large middle and small ends.

(**a**)

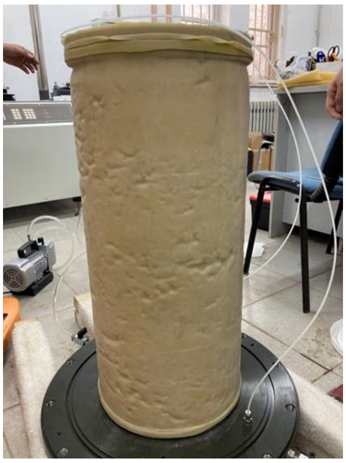

(**b**)

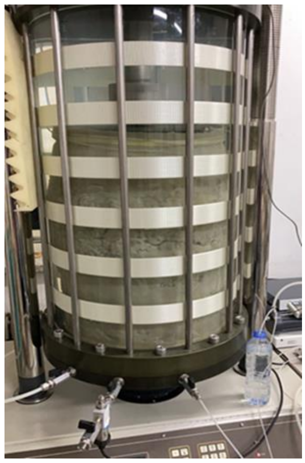

(**c**)

Figure 4. Triaxial compression test process (**a**) specimen fabrication (**b**) specimen before test (**c**) specimen after test.

The stress–strain relationship is illustrated in Figure 5. Throughout the test, it was observed that the stress increased with increasing axial strain, exhibiting a clear parabolic relationship. A peak value of the stress–strain curve occurred at an axial strain of approximately 4%, suggesting that the specimen had undergone shear failure at this point. Following the peak value, the shear stress started to decrease as the axial strain continued to increase, demonstrating strain softening behavior. The peak strength obtained from the test was 588 kPa and the value of E_{50}, calculated using the aforementioned method, was 409 kPa.

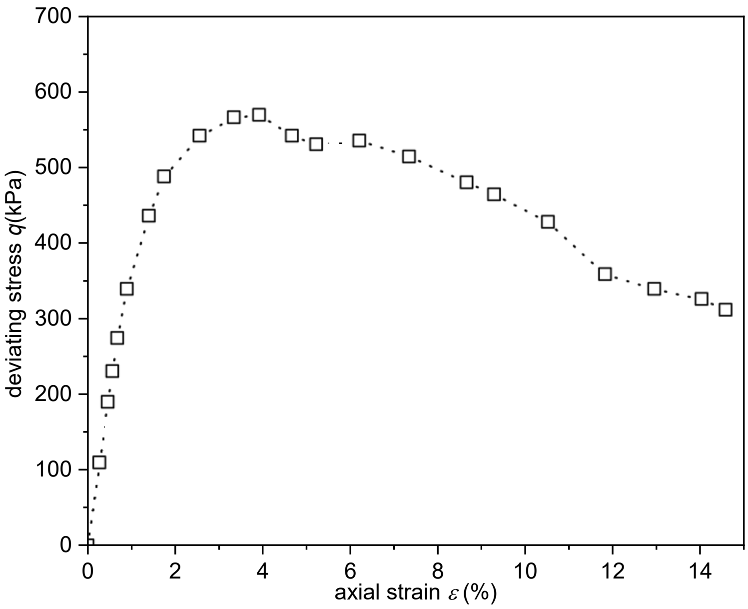

Figure 5. 100 kPa undisturbed stress–strain curve.

The consolidated drained shear tests were conducted on the soil sample to determine its internal friction angle and cohesion. The tests were performed with confining pressures of 200 kPa and 300 kPa. At confining pressures of 100 kPa, 200 kPa, and 300 kPa, the maximum principal stress was recorded as 688 kPa, 1212 kPa, and 1635 kPa, respectively. The calculations indicated that the soil cohesion was 48.1 kPa and the internal friction angle was 36.5°.

2.3. Loading and Unloading Triaxial Compression Test

As mentioned before, to obtain the unloading-reloading Young's modulus of sandy gravel soil, it is necessary to conduct a loading-unloading triaxial compression test on the sample when the confining pressure is 100 kPa. By calculating the average slope of the hysteresis loop formed during the loading and unloading process, the unloading-reloading Young's modulus E_{ur} can be obtained.

There are four main steps of a loading and unloading triaxial compression test. The first three steps are sample installation, saturation, and consolidation, the same as the triaxial compression test. After that, unloading and reloading shall be carried out. The load applied for the first time is 25% of the failure stress of the sample. When the load approaches the target value, the unloading shall be carried out immediately until the load is about 0, and then reload 50% of the expected failure stress onto the sample. In order to better control the value of the applied load, stress control is used in all loading and unloading processes. The whole test process is shown in Figure 6.

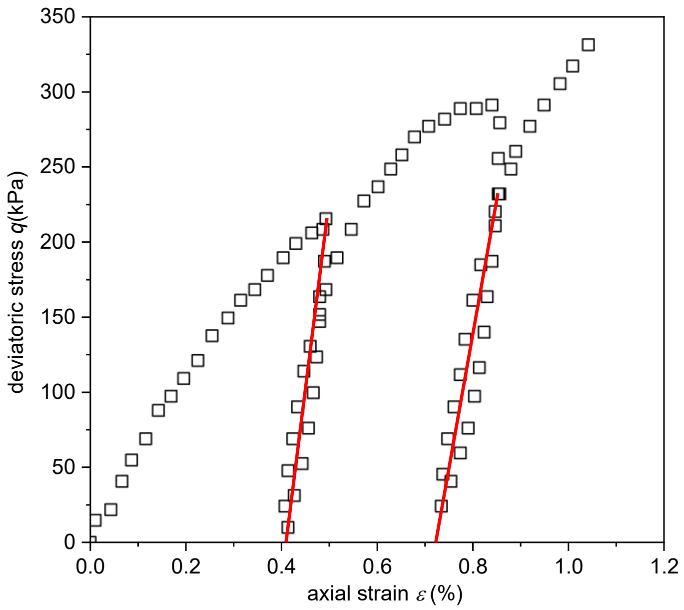

Figure 6. Loading-unloading-reloading experimental curve of sandy gravel.

As shown in Figure 6, when the soil sample is unloaded, the trend of the stress–strain curve varies from steep to slow, indicating that the soil sample has undergone a certain degree of plastic deformation at this time. When the soil sample is reloaded, the curve trend is the same as during unloading. Two unloading-reloading processes are carried out during the test; the average value of their slopes is the E_{ur} of the sample, and it is calculated that E_{ur} = 1851 kPa.

2.4. Standard Consolidation Test

There is little research on the standard consolidation test of coarse-grained soil in China, and most scholars focus on isobaric consolidation. However, the standard consolidation test is one of the necessary tests to study the HS model. In this paper, a large-scaled consolidator (Figure 7) with a 300 mm diameter is used to measure the relationship between the deformation and pressure of a sandy gravel soil sample by a standard consolidation test. The stress–strain curve under lateral limit conditions is obtained, and the oedometric loading Young's modulus E_{oed} can be calculated.

Figure 7. Large-scaled consolidator.

The soil sample was subjected to five incremental axial loads of 50, 100, 200, 400, and 800 kPa, respectively, after saturation. A consolidation time of 24 h was allocated for each loading level. The deformation was considered to have reached completion when the hourly axial displacement was less than 0.01 mm/min under each loading level, at which point the next load level was applied until the completion of the test. The resulting stress–strain relationship was documented in Figure 8.

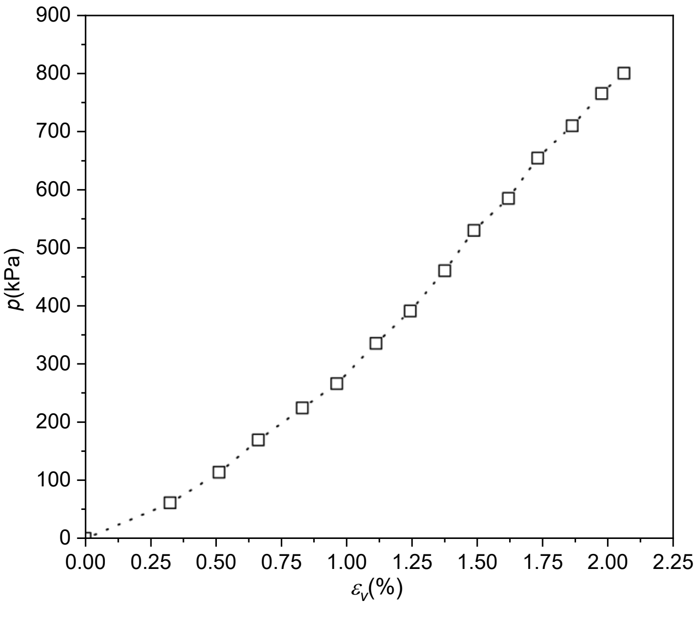

Figure 8. Curve of standard consolidation test of sandy gravel soil sample.

The axial strain of soil under lateral confinement exhibits an exponential increase in response to the applied stress, primarily due to the limited ability of soil volume to decrease as soil porosity decreases during the compression process. The oedometric loading Young's modulus can be determined by the slope of the tangent at a specific point on the stress–strain curve, with the axial stress being 100 kPa. In this test, the obtained modulus value was found to be 424 kPa. The results of the triaxial drained shear test, loading-unloading-reloading test, and standard consolidation test were analyzed to determine the proportional relationship between three stiffness parameters of the HS model. The findings indicate that the proportion is E_{oed}:E_{50}:E_{ur} = 1:1:4.3.

3. Numerical Simulation Verification

Based on a foundation pit project in Beijing, the geotechnical finite element software MIDAS GTS is used for simulation. In this part, taking the surface settlement and support structure deformation as indicators, the simulated results are compared with the field monitoring values to verify the proportional relationship between the stiffness parameters of the sandy gravel HS model in the Beijing area.

3.1. Model Parameters

The project's construction land covers 8913 m^2, with a length of about 120 m and a width of about 60 m. It has four floors underground, and the buried depth of the foundation is about 17.70 m. This paper's constitutive models of the soil layers are all HS models. According to the survey report and the actual excavation on site, the soil is divided into eight layers from top to bottom. The specific parameters of each layer are shown in Table 3. Among them, the sandy gravel parameters of the fifth and seventh layers are calculated according to E_{oed}:E_{50}:E_{ur} = 1:1:4.3.

Table 3. Physical and mechanical parameters of different soil layers.

Soil Layer	Thickness (m)	Gravity (m)	Cohesion (kPa)	Internal Friction Angle (Rad)	Poisson's Ratio	E_{50} (MPa)	E_{oed} (MPa)	E_{ur} (MPa)
Miscellaneous fill	4	16.5	5	10	0.35	13	13	52
Sandy silt	3	21	0	15	0.29	10	10	40
Clay	2	18.8	21	12	0.31	6	6	30
Fine sand	5	19.8	0	28	0.27	20	20	60
Sandy gravel	7	21.2	0	35	0.23	30	30	129
Silt	2	14	15	25	0.37	14	14	56
Sandy gravel	8	21.5	0	40	0.21	40	40	172
Silty clay	3	19.2	27.2	13.9	0.357	12	12	48

The boundary of the model should be 3~5 times the depth of the foundation pit, so the length × width × depth is 400 m × 200 m × 80 m, respectively. Based on the conditions, a three-dimensional stratum structure model is established. The whole model has 350,693 nodes and 268,479 units. The structural models of the foundation pit, stratum, and surface buildings are shown in Figure 9.

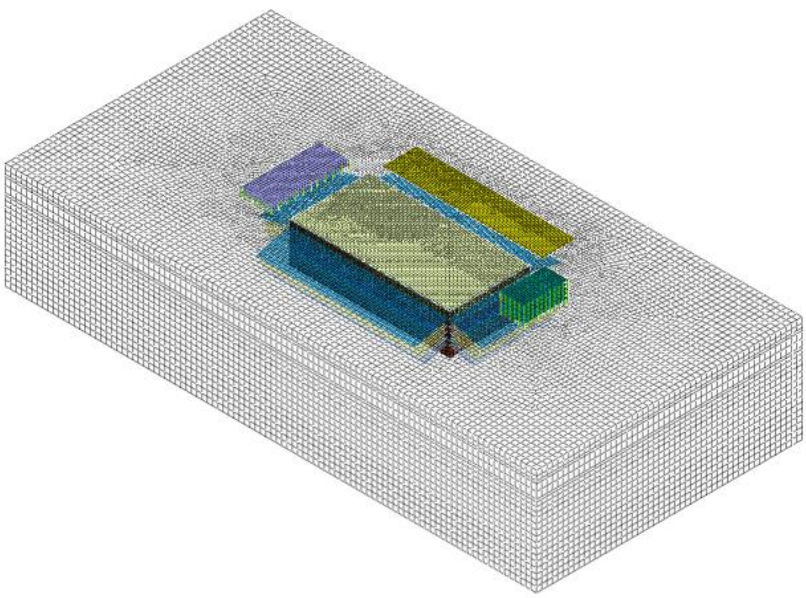

Figure 9. The finite element model of the foundation pit.

In this part, the boundary around the model restricts the normal displacement, and the vertical displacement is free. The bottom is a fixed boundary condition, and the top soil layer is set as a free boundary. At the same time, in order to ensure that the model is closer to the actual site construction conditions, the precipitation step is added to the model. An initial pressure head is applied to the surface around the soil at −19 m of the stratum; a pressure head of 0 is applied at −30 m of the excavated soil of the foundation pit as the dewatering head. Existing buildings around the pit are transformed into an equivalent load. The structural load of the two-story is 1687.5 kN, and the structural load of the five-story is 4218.75 kN. The buildings west of the pit are simplified as a uniformly distributed load, which is 843.75 kN.

3.2. Simulation Results

In the present project, a foundation pit with a depth of 25 m was excavated in six increments. The support structure was implemented in a timely manner following each excavation stage. The excavation process resulted in soil unloading, causing a settlement of the soil outside the pit, as well as horizontal displacement of the retaining structure. The correlation between surface settlement and deformation of the retaining structure remains a crucial aspect of foundation pit excavation research. In this study, numerical simulation results were compared to field monitoring data to verify the proportionality of the critical stiffness parameters in the HS model.

3.2.1. Comparative Analysis of Surface Subsidence

Figure 10 shows the comparison of surface deformations under each excavation step. The abscissa is the distance between the measuring point and the edge of the foundation pit, and the ordinate is the corresponding surface settlement value. The shape of the settlement curve indicates that the displacement of the soil surrounding the excavation site initially increases and then decreases as the distance from the pit increases. The depth of the excavation has a significant impact on the position of the maximum settlement point, which shifts away from the edge of the pit as the excavation depth increases. Upon completion of excavation, the location of the maximum settlement point is approximately 25 m from the edge of the excavation site. It can be seen that, although there are some differences between the numerical simulation results and the monitoring values, the overall deformation tendency is the same. The correlation coefficients are 0.95~0.99, and the average standard deviations are 0.005~0.134. Figure 11 shows the settlement values of key measuring points under different excavation steps. With the increase in excavation depth, the settlement value gradually increases, and the difference between the numerical simulation value and the actual monitoring value is slight. This shows that the numerical simulation effectively predicts the settlements of the actual project.

3.2.2. Comparative Analysis of Horizontal Deformation of Enclosure Pile

The results of numerical simulation and field monitoring are presented in Figure 12 to evaluate the horizontal deformation of the retaining pile. The horizontal displacement of the retaining pile is plotted on the abscissa, while the depth of the retaining pile is plotted on the ordinate. The deformation at the top of the pile is the largest, and gradually decreases with increasing depth. The results of the numerical simulation are in good agreement with the field monitoring data, with a slight difference observed near the surface. The maximum deformation values obtained from both the numerical simulation and field monitoring are located at the top of the enclosure pile. The maximum deformation value obtained from the finite element calculation is 16.35 mm, while the maximum value obtained from site monitoring is 18.36 mm.

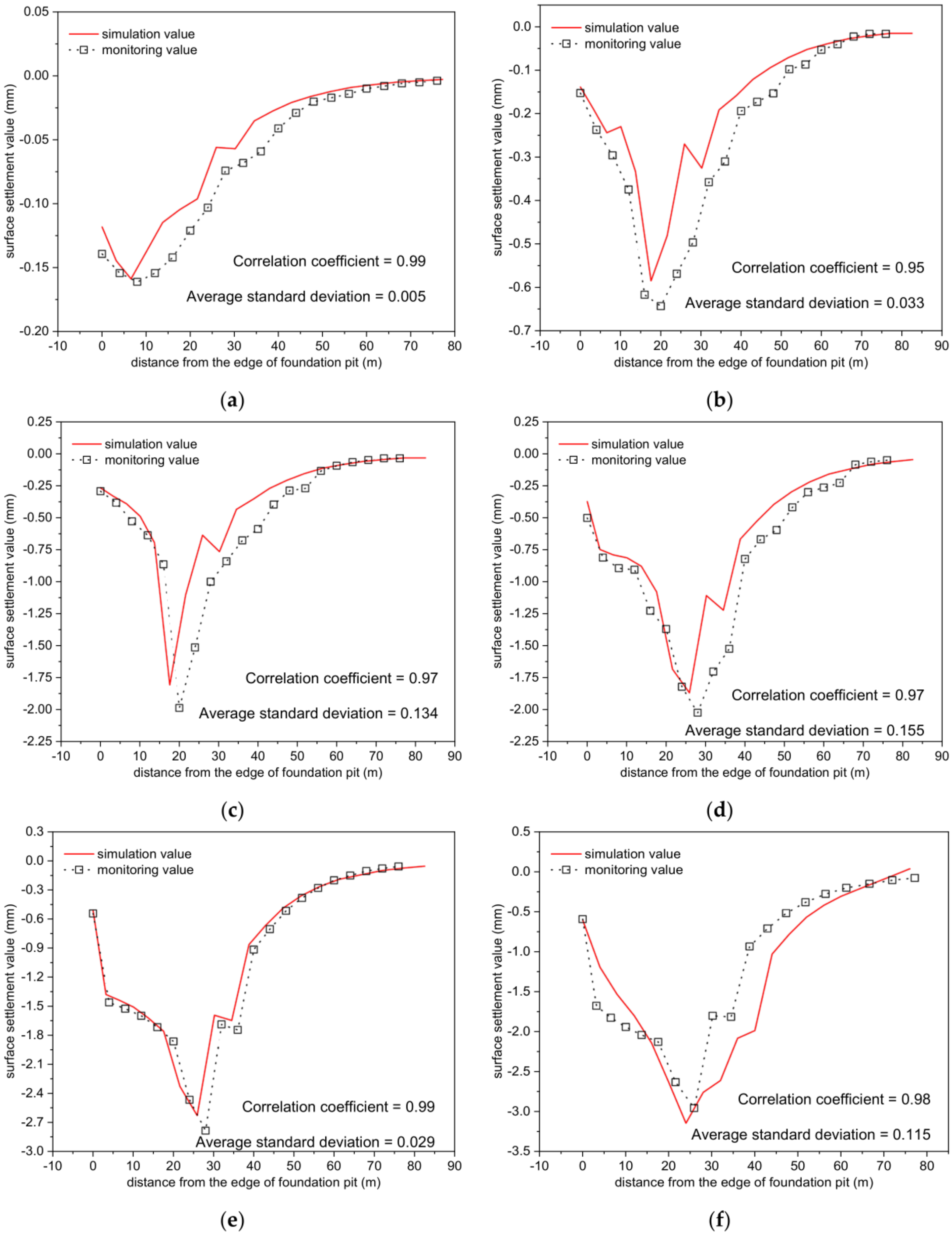

Figure 10. Comparison of surface settlement value under various excavation conditions. (**a**) step 1; (**b**) step 2; (**c**) step 3; (**d**) step 4; (**e**) step 5; (**f**) step 6.

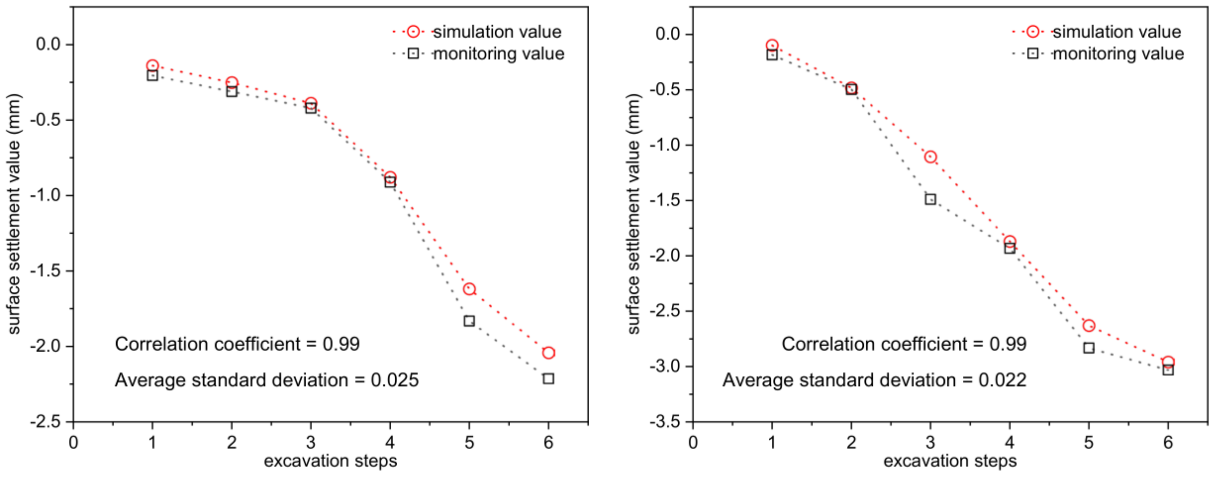

(a) (b)

Figure 11. Comparison of surface settlement values of key monitoring points. (**a**) key point 1; (**b**) key point 2.

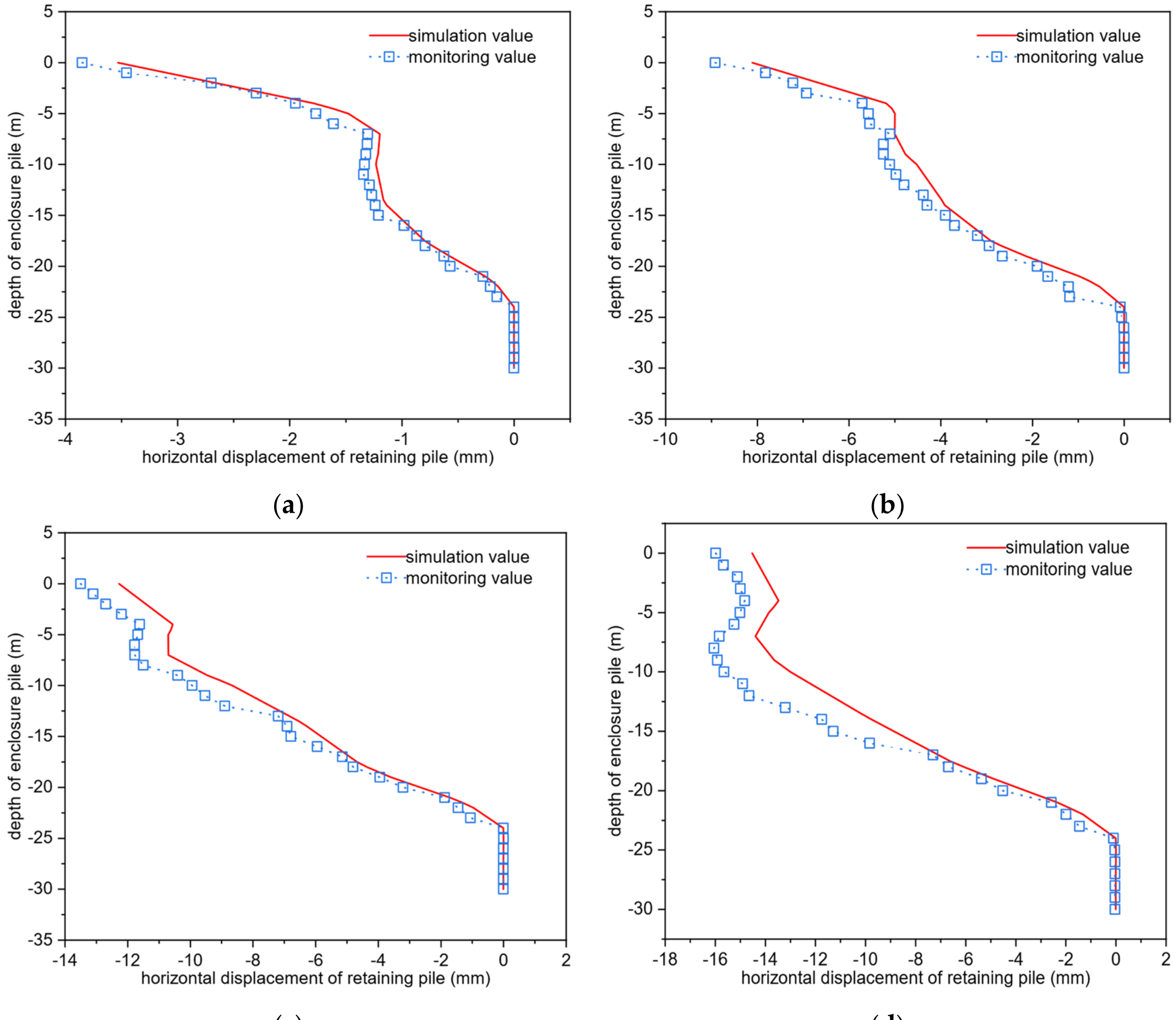

(a) (b) (c) (d)

Figure 12. *Cont.*

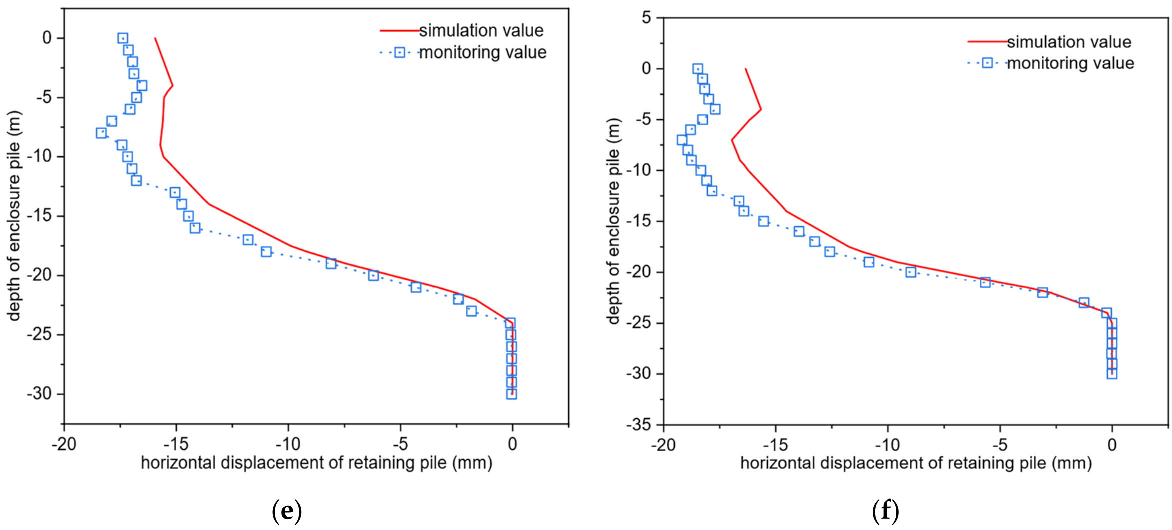

Figure 12. Comparison of horizontal deformation of retaining piles in different steps. (**a**) step 1; (**b**) step 2; (**c**) step 3; (**d**) step 4; (**e**) step 5; (**f**) step 6.

3.3. Validation Analysis

The comparison of the surface settlement and horizontal deformation of the support structure between the results of numerical simulation and field monitoring data exhibits a comparable tendency. The observed values in the field tend to be larger, primarily due to the presence of additional loads such as construction machinery and materials during the actual project implementation. This discrepancy can be attributed to several factors including site piling, the presence of construction vehicles, and the premature installation of prestressing anchors during construction. Nevertheless, it is believed that the results of numerical simulations can, to a certain extent, represent the actual monitoring values, thereby reinforcing the accuracy of the obtained proportional relationship of the stiffness in this study.

4. Conclusions

The hardening soil model (HS model) considers shear hardening and compression hardening in the simulation process and has certain advantages in numerical simulation. This study conducted large-scale mechanical experiments to test the E_{50}, E_{oed}, and E_{ur} of sandy gravel, which were the key stiffness parameters of the HS model. The proportional relationship of these parameters was proposed. The validity of the established stiffness ratio relationship was verified through numerical simulations of a foundation pit project and comparison with field monitoring data. The main findings of this study are as follows:

(1) The large sandy gravel samples with 600 mm height and 300 mm diameter were prepared to conduct a large-scale triaxial drained shear test, an unloading-reloading test, and a standard consolidation test.

(2) For sandy gravel stratum, the Young's moduli under triaxial loading (E_{50}), oedometric loading (E_{oed}), and unloading-reloading (E_{ur}) were tested. The proportion of the three stiffness parameters was found to be E_{oed}:E_{50}:E_{ur} = 1:1:4.3.

(3) The numerical calculations and field monitoring values showed a similar tendency, suggesting that the simulation results can accurately represent the actual monitoring values. This supports the validity of the stiffness proportion relationship established in this study.

(4) The primary contribution of this work is the proposal of a novel method for determining the parameters of the HS model for the sandy gravel stratum. The conclusions can be applied to theoretical studies and numerical simulations of similar engineering. It is suggested that follow-up studies can be carried out for sandy gravel with different compositions to obtain more universal conclusions.

Author Contributions: Conceptualization, X.S.; methodology, J.S. and Y.Q.; software, X.Z. (Xueming Zhang); validation, R.L. and H.C.; formal analysis, X.S.; investigation, X.Z. (Xiangyang Zhu); resources, X.Z. (Xiangyang Zhu); data curation, Y.Q.; writing—original draft preparation, Y.Q.; writing—review and editing, J.S. and X.S.; visualization, X.Z. (Xueming Zhang); supervision, X.S.; project administration, J.S.; funding acquisition, X.S. All authors have read and agreed to the published version of the manuscript.

Funding: This work is supported by the Talent Fund of Beijing Jiaotong University (Grant No. 2021RC226) and the Beijing Natural Science Foundation for Young Scientists (Grant No. 8214052).

Institutional Review Board Statement: Not applicable.

Informed Consent Statement: Not applicable.

Data Availability Statement: The data are available from the corresponding author on reasonable request.

Conflicts of Interest: The authors declare no conflict of interest.

References

1. Murthy, V.N.S. *Geotechnical Engineering*; Marcel Dekker: New York, NY, USA, 2003.
2. Ishibashi, I.; Hazarika, H. *Soil Mechanics Fundamentals and Applications*, 2nd ed.; Taylor & Francis Group: Abingdon, UK, 2015.
3. Bolton, M.D. The strength and dilatancy of sands. *Géotechnique* **1986**, *36*, 65–78. [CrossRef]
4. Evans, M.D.; Zhou, S. Liquefaction behavior of sand-gravel composites. *J. Geotech. Eng. ASCE* **1995**, *121*, 287–298. [CrossRef]
5. Rollins, K.M.; Evans, M.D.; Diehl, N.B.; Daily, W.D., III. Shear modulus sand damping relationships for gravels. *J. Geotech. Geoenvironmental Eng. ASCE* **1998**, *124*, 396–405. [CrossRef]
6. Cetin, H.; Fener, M.; Gunaydin, O. Geotechnical Properties of tire-cohesive clayey soil mixtures as a fill material. *Eng. Geol.* **2006**, *88*, 110–120. [CrossRef]
7. El Dine, B.S.; Dupla, J.C.; Frank, R.; Canou, J.; Kazan, Y. Mechanical characterization of matrix coarse-grained soils with a large-sized triaxial device. *Can. Geotech. J.* **2010**, *47*, 425–438. [CrossRef]
8. Lirer, S.; Flora, A.; Nicotera, M.V. Some remarks on the coefficient of earth pressure at rest in compacted sandy gravel. *Acta Geotech.* **2011**, *6*, 1–12. [CrossRef]
9. Duncan, J.M.; Chang, C.Y. Nonlinear Analysis of Stress-strain in Soils. *J. Soil Mech. Found. Div.* **1970**, *96*, 1629–1653. [CrossRef]
10. Schanz, T.; Vermeer, P.A.; Bonnier, P.G. The Hardening Soil Model: Formulation and Verification. In *Beyond 2000 in Computational Geotechnics*; Balkema: Rotterdam, The Netherlands, 1999; pp. 281–297.
11. Schweiger, H.F.; Vermeer, P.A.; Wehnert, M. On the design of deep excavations based on finite element analysis. *Geomech. Tunn.* **2009**, *2*, 333–344. [CrossRef]
12. Blackburn, J.T. *Automated Remote Sensing and Three Dimensional Analysis of Internally Braced Excavations*; Northwestern University: Evanston, IL, USA, 2005.
13. Finno, R.J.; Calvello, M. Supported Excavations: Observational method and inverse modeling. *J. Geotech. Geoenviron. Eng. ASCE* **2005**, *7*, 826–836. [CrossRef]
14. Wu, K.; Shao, Z.S.; Jiang, Y.L.; Zhao, N.N.; Qin, S.; Chu, Z.F. Determination of stiffness of circumferential yielding lining considering the shotcrete hardening property. *Rock Mech. Rock Eng.* **2023**, *56*, 1–12.
15. Sanglerat, G. *The Penetrometer and Soil Exploration*; Elsevier Publishing Company: Amsterdam, The Netherlands, 1972.
16. Schanz, T.; Vermeer, P.A. *On the Stiffness of Sands. Pre-failure Deformation Behaviour of Geomaterials*; Thomas Telford Publishing: London, UK, 1998; pp. 383–387.
17. Ng, C.W.W. *An evaluation of Soil-Structure Interaction Associated with a Multi-Propped Excavation*; University of Bristol: Bristol, UK, 1992.
18. Ou, C.Y.; Shiau, B.Y.; Wang, I.W. Three-dimensional deformation behavior of the Taipei National Enterprise Center (TNEC) excavation case history. *Can. Geotech. J.* **2000**, *37*, 438–448. [CrossRef]
19. Janbu, J. Soil compressibility as determined by oedometer and triaxial tests. *Proc. European Conf. SMFE* **1963**, *1*, 19–25.
20. Brinkgreve, R.B.J.; Broere, W. *Plaxis Material Models Manual*; Delft University of Technology: Delft, The Netherlands, 2006.
21. Calvello, M.; Finno, R.J. Selecting parameters to optimize in model calibration by inverse analysis. *Comput. Geotech.* **2004**, *31*, 411–425. [CrossRef]
22. Liu, X.D. On HSS Model Application in Ground Settlement Calculation of Shield Tunneling. *Journal of Municipal Technology.* **2020**, *4*, 119–123.
23. Wang, W.D.; Wang, H.R.; Xu, Z.H. Experimental study of parameters of hardening soil model for numerical analysis of excavations of foundation pits. *Rock Soil Mech.* **2012**, *8*, 2283–2290.
24. Yang, L.Q.; Zhou, L.B.; Xia, W.; Guan, R.Q.; Zhang, H.; Luo, W.J. Experimental Study of Parameters of HS Model for Numerical Analysis of Foundation Pits in Ningbo Soft Soil Area. *Tunn. Constr.* **2018**, *38*, 954–962.
25. Pang, X.C.; Huang, J.J.; Su, D.; Xiao, W.H.; Gu, W.T.; Liu, B. Experimental study on parameters of the hardening soil model for undisturbed granite residual soil in Shenzhen. *Rock Soil Mech.* **2018**, *39*, 4079–4085.

26. Hsieh, P.; Ou, C.; Lin, Y. Three-dimensional deformation behavior of the Taipei National Enterprise Center (TNEC) excavation case history. *J. Geotech. Geoenviron. Eng.* **2013**, *8*, 33–48.
27. Schweiger, H.F.; Scharinger, F.; Lüftenegger, R. 3D finite element analysis of a deep excavation and comparison with in situ measurements. In *Geotechnical Aspects of Underground Construction in Soft Ground*; Taylor & Francis Group: London, UK, 2009; pp. 193–199.
28. Roboski, J.F. *Soil Parameters for Constitutive Models of Compressible Chicago Glacial Clays*; Northwestern University: Evanston, IL, USA, 2001.
29. Zhang, L.F.; Zhou, G.C. Parameters Selection and Sensitivity Analysis of Settlement of Silt Seawall Based on Hardened Soil Model. *Water Resour. Power* **2019**, *37*, 85–87+91.